ECAS 2022

MDPI

Proceeding Paper

Estimations of CO and NO_2 Emissions and the Fire Combustion Efficiency for Fire Activities over CONUS Using TROPOspheric Monitoring Instrument (TROPOMI) Measurements †

Wei-Ting Hung [1,2,*], Barry Baker [1], Patrick Campbell [1,2], Youhua Tang [1,2] and Gill-Ran Jeong [1,2]

[1] Air Resources Laboratory, National Oceanic and Atmospheric Administration, MD, USA; barry.baker@noaa.gov (B.B.); patrick.c.campbell@noaa.gov (P.C.); youhua.tang@noaa.gov (Y.T.); gjeong@gmu.edu (G.-R.J.)

[2] Center for Spatial Information Science and Systems, George Mason University, VA, USA

* Correspondence: whung@gmu.edu

† Presented at the 5th International Electronic Conference on Atmospheric Sciences, 16–31 July 2022; Available online: https://ecas2022.sciforum.net.

Abstract: This study quantifies the carbon monoxide (CO) and nitrogen dioxide (NO_2) emissions (E_{CO} and E_{NO2}) from fire activities over the contiguous United States (CONUS) in 2020 using the total-column CO and NO_2 measurements from the TROPOspheric Monitoring Instrument (TROPOMI) satellite. The contributions of local emissions, atmospheric transport, chemical loss, and averaging kernel are considered. The emission ratio (ER = E_{NO2}/E_{CO}) is used as a proxy of fire combustion efficiency. Preliminary results show that, TROPOMI E_{CO} shows a similar seasonal variation to fire emission inventories with significant enhancements during summertime while TROPOMI E_{NO2} shows an opposite trend. TROPOMI ER also shows a significant seasonal variation, introducing the capability of attributing fire seasons associated with different fire and land types.

Keywords: fire emission; combustion efficiency; TROPOMI

Academic Editor(s): Anthony Lupo

Published: 14 July 2022

1. Introduction

Fire activities, including wildfires and prescribed fires, are one of the important sources of trace gases and aerosols in the US. Wildfires primarily occur in the western states during summer and fall associated with forest fires [1]. Prescribed fires, including agricultural and deforestation burnings, occur over the southeastern US in winter and the central US during springtime mainly associated with savanna and rangeland fires [1]. Prescribed fires are commonly used for land management and could reduce the impacts of wildfires by consuming accumulated fuels [2,3]. Also, prescribed fires are usually better managed under specific meteorological conditions (e.g., air temperature less than 80 °F/27 °C) and are less intense compared to wildfires.

Most of the current fire emission inventories estimate fire emissions based on total burned area, fuel loadings, fractions of burned fuels, and compound-specific emission factors. The uncertainties of estimation of burned loadings and assumptions of compound-specific factors lead to various results from different emission inventories. Recently, the total-column CO and NO_2 measurements from TROPOMI, launched in October 2017, are often used for the estimation of anthropogenic and fire emissions [4–6]. The state-of-the-art techniques, daily global coverage, and fine spatial resolution offer the opportunity to directly estimate fire emissions from space. Also, the ratio of NO_2 and CO emissions could

be used as a proxy of fire combustion efficiency and is able to identify the spatiotemporal variabilities of fire characteristics [7,8].

In this study, the total-column CO and NO_2 measurements from TROPOMI are used to quantify the daily CO and NO_2 fire emissions (E_{CO} and E_{NO2}) and emission ratio (ER = E_{NO2}/ E_{CO}) over CONUS in 2020. Results are compared with five fire emission inventories, including the preliminary 2020 National Emissions Inventory (NEI) from the United States Environmental Protection Agency (US EPA) (https://www.epa.gov/air-emissions-inventories/2020-national-emissions-inventory-nei-documentation), the Blended Global Biomass Burning Emissions Product (GBBEPx) [9], the Fire INventory from NCAR (FINN) [10], the Global Fire Assimilation System (GFAS) [11], and the Quick Fire Emissions Dataset (QFED) [12].

2. Datasets and Methods

2.1. Data Selection

TROPOMI CO and NO_2 measurements with quality flag larger than 0.7 and 0.75, respectively, are selected for clear and thin cloud conditions. Measurements over snow- and ice-covered surface are removed. These measurements are further gridded to 0.1 × 0.1 degree to be consistent with emission inventories. Additionally, to remove the influence of local emissions from sources other than fire activities, the annual median values (X_{annual}) of no-fire days (days without fire records) at each grid are determined and subtracted from the measurements ($X_{measure}$).

Fire points, reported in EPA NEI, with fire radiative power (FRP) from GBBEPx exceeding the 95th percentile (~65 MW) are selected to focus on well-identified fire activities. These fire points are categorized into 10 regions according to the US EPA regional offices (https://www.epa.gov/aboutepa/regional-and-geographic-offices). Inventory NOx and NO emissions, except for FINN, are converted into NO_2 emissions by using a ratio of NO:NO_2 of 85:15 [13,14]. Note that, although EPA NEI reports near-surface fire emissions in tons, they are expected to be correlated with satellite-based and inventory emissions.

2.2. Emission Estimation

Based on Lama et al. (2020) [7] and van der Velde et al. (2021) [8], E_{CO} and E_{NO2} are calculated as:

$$E_i = \Delta X_i \times \frac{U}{L} \times K_i[OH]\ [mol\ cm^2 s^{-1}] \quad (1)$$

$$K_{CO} = 1.1 \times 10^{-12} \times (\frac{T}{300})^{1.3}\ [cm^3 mol^{-1} s^{-1}] \quad (2)$$

$$K_{NO2} = 2.8 \times 10^{-11}\ [cm^3 mol^{-1} s^{-1}] \quad (3)$$

where i refers to CO and NO_2, X is the total-column density after subtracting annual medians ($X = X_{measure} - X_{annual}$), U and T are the integrated wind speed and air temperature from the surface to 7000 m a.g.l. from the High-Resolution Rapid Refresh (HRRR; https://rapidrefresh.noaa.gov/hrrr/), L is the diameter of the fire center which is 0.1 degree (~ 11 km) in this study, K_i is the X_i-OH reaction rates reported in Burkholder et al. (2015) [15], and [OH] is the OH column-average concentration within the planetary boundary layer (PBL) which is 1.5×10^7 mol cm^{-3} [7] in this study. In Equation (1), the term ΔX represents the difference between fire areas (X_{fire}) and the background ($X_{background}$). The terms U/L and K_i[OH] represent the effect of atmospheric transport and chemical loss, respectively. To determine X_{fire} and $X_{background}$ for CO, a 5 × 5 degree fire box with fire point as the center and a 3 × 3 degree upwind box are selected. The upwind box is determined by the skirt distance (5 + 3 degree) and column-average horizontal wind from the surface to 7000 m a.g.l., which is assumed to be consistent during the day. As for NO_2, since NO_2 has a

relatively short lifetime (3–10 h) and is less affected by atmospheric transport, a 3 × 3 degree fire box is used while the size of upwind box and skirt distance are the same as CO. For each selected fire point, X_{fire} and $X_{background}$ are calculated as the averages of fire and upwind boxes, respectively.

The averaging kernel (A) is often used in the satellite retrieval processes to describe the sensitivity of total-column measurement to the changes in vertical profile. The application of A could strongly affect the result of satellite retrievals. Thus, to compare with emission inventories, TROPOMI ER is corrected by taking satellite averaging kernel into account:

$$ER = \frac{E_{NO2}}{E_{CO}} \frac{1}{(1 - A_{influence})} \quad (4)$$

where $A_{influence}$ states for the influence of satellite averaging kernel, which is 9% adopted from Lama et al. (2020) [7].

3. Preliminary Results

3.1. Comparison between TROPOMI and Emission Inventories

TROPOMI E_{CO}, E_{NO2} and ER are compared with five fire emission inventories (EAP NEI, GBBEPx, FINN, GFAS, and QFED). To reduce the uncertainties due to atmospheric transport, regional daily averages of E_{CO}, E_{NO2} and ER are calculated assuming that nearby fires share the same fire characteristics. Overall, TROPOMI emissions are much lower than emission inventories, except for EPA NEI. For E_{CO} (Figure 1(a-1)), GBBEPx, FINN, GFAS, and QFED are on average 20.5, 25.7, 3.8 and 5.8 times of TROPOMI, respectively. TROPOMI E_{CO} shows moderate linear correlations with emission inventories with correlation coefficients (Rs) around 0.3. Also, a clear seasonal variation is found for all datasets (Figure 1(a-2)) with significant enhancements during summer.

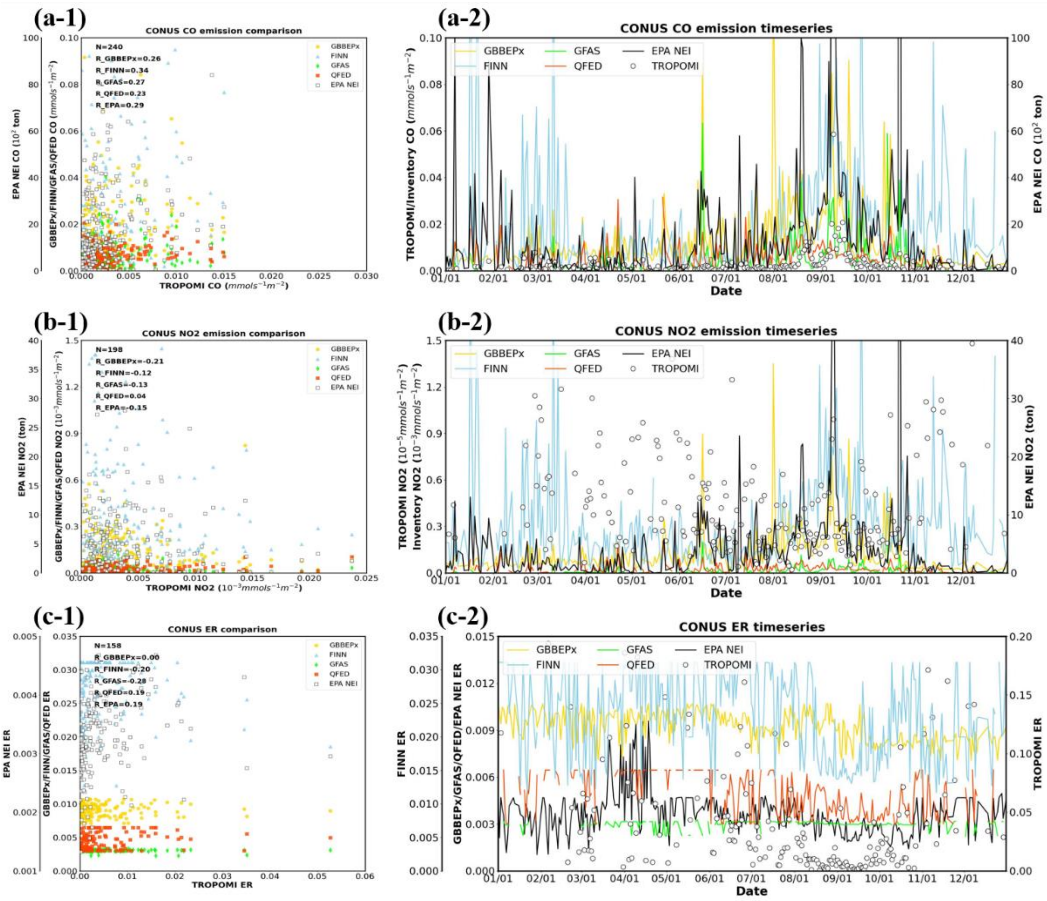

Figure 1. Scatter plots and timeseries of (**a**) E_{CO}, (**b**) E_{NO2}, and (**c**) ER of TROPOMI and five fire emission inventories. Colors state for different data sources.

For E_{NO2} (Figure 1(b-1)), GBBEPx, FINN, GFAS, and QFED are on average 124.5, 239.7, 9.0 and 15.1 times of TROPOMI, respectively. TROPOMI shows negative correlations with GBBEPx, FINN and GFAS with Rs around −0.1–−0.2, and nearly no correlation with QFED with a R of 0.04. Inventory E_{NO2}s share a similar seasonal variation with E_{CO}s (Figure 1(b-2)), as they are estimated by assigning burned fractions in total biomass loading for different species. However, TROPOMI E_{NO2} does not show such variation and is even slightly lower during summertime, which is opposite to E_{CO}. It is probably because of the higher NO_2 background level during summer due to increasing anthropogenic and biogenic NOx emissions at high temperatures [16]. Since the emission estimation used in this study is based on the differences between fire regions and the background, a high background level could make such differences less significant, leading to an underestimation of E_{NO2}.

As for ER (Figure 1(c-1)), inventory ERs fall in specific ranges probably due to the prescribed emission factors used in emission estimation. For instance, QFED ER shows a range of 0.003–0.006, corresponding to the ratios of NO_2 to CO emission factors which are 0.002 and 0.006 for tropical forest and savanna, respectively [12]. In addition, affected by the seasonal variation of E_{CO} and E_{NO2}, TROPOMI ER is higher during March–June and significantly lower in August and September (Figure 1(c-2)), showing the capability of distinguishing different fire seasons. Although the ERs are relatively consistent compared to TROPOMI, FINN, QFED, and EPA NEI also show a similar seasonal variation to TROPOMI with the lowest ERs during summer.

3.2. Capability of TROPOMI ER of Distinguishing Fire and Land Types

To further investigate the capabilities of TROPOMI ER, results for two fire types identified in EPA NEI, wildfire and prescribed fire, and four land types identified in QFED, tropical forest (TF), extratropical forest (XF), savanna (SV), and grassland (GL), are analyzed.

Figure 2a illustrates the boxplots of TROPOMI E_{CO}, E_{NO2} and ER for different fire types. The averages of E_{CO} and E_{NO2} for wildfire (prescribed fire) are 0.009 ± 0.015 mmol m^{-2} s^{-1} (0.003 ± 0.003 mmol m^{-2} s^{-1}) and 0.004 ± 0.004 × 10^{-3} mmol m^{-2} s^{-1} (0.018 ± 0.013 × 10^{-3} mmol m^{-2} s^{-1}), respectively. These results are consistent with previous studies with higher E_{CO} and lower E_{NO2} for wildfire compared to prescribed fire [17–19]. Although the average E_{CO} for wildfire is 3-folds of prescribed fire, the medians for two fire types are comparable (0.004 mmol m^{-2} s^{-1} for wildfire and 0.003 mmol m^{-2} s^{-1} for prescribed fire), indicating a similar base condition of two fire types and the possible contribution of extreme wildfire events. The high E_{NO2} for prescribed fire may partly be due to the larger fraction of smoldering combustions compared to wildfire. According to Lobert and Warnatz (1993) [13], NO_2 contributes up to 40% of total NOx emissions in smoldering combustions, and around 14% in flaming combustions which are dominant in wildfires. However, the difference of the contributions of CO in total carbon emissions in two combustions is less significant (2–15%), resulting in a relatively small difference of E_{CO} between two fire types. Moreover, ER is lower for wildfire with an average of 0.003 ± 0.008 and higher for prescribed fire with an average of 0.017 ± 0.048, introducing a good capability of distinguishing two fire types.

Figure 2b illustrates the boxplots of TROPOMI E_{CO}, E_{NO2} and ER for the four land types defined in QFED. Since there is no TF identified over CONUS, only XF, SV and GL are discussed here. Overall, XF shows higher E_{CO} and lower E_{NO2} with averages of 0.011 ± 0.017 mmol m^{-2} s^{-1} and 0.005 ± 0.004 × 10^{-3} mmol m^{-2} s^{-1}, respectively. GL shows the lowest E_{CO} and the highest E_{NO2} with averages of 0.004 ± 0.005 mmol m^{-2} s^{-1} and 0.010 ± 0.010 × 10^{-3} mmol m^{-2} s^{-1}, respectively. This is consistent with the emission factors used in the selected emission inventories [9–12] and reported in previous studies [20,21]. Laboratory

experiments also found higher E_{CO} and lower E_{NO2} for boreal forest fires compared to grassland fires [22]. Therefore, XF shows the lowest ER while GL shows the highest ER with averages of 0.002 ± 0.003 and 0.019 ± 0.079, respectively, indicating the potential of ER of identifying different land types. Note that the land type categorization does not consider fire types. For instance, GL fires could be actually a combination of wildfires and prescribed fires. It may introduce uncertainties to the land type identification merely based on TROPOMI ER.

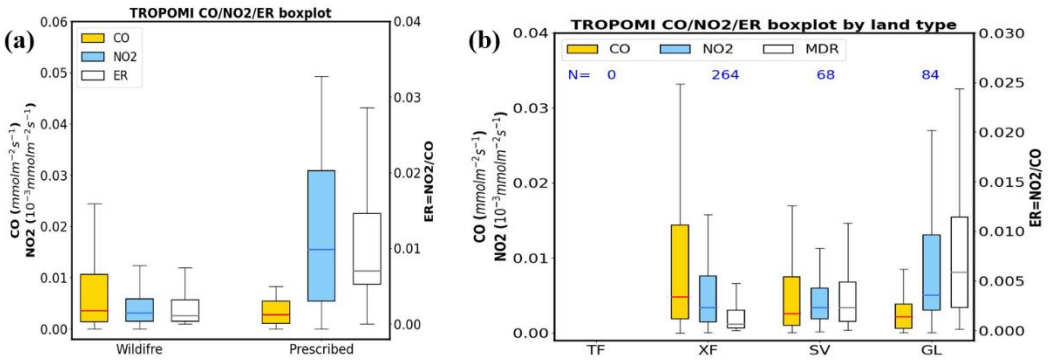

Figure 2. Boxplots of ECO, E_{NO2} and ER associated with (**a**) two fire types and (**b**) four land types.

4. Conclusions

This study estimates CO and NO_2 fire emissions and uses emission ratio (ER) as the proxy of combustion efficiency using the total-column CO and NO_2 measurements from TROPOMI over CONUS in 2020. Preliminary results show that TROPOMI E_{CO} and E_{NO2} are 4–26 and 9–240 times lower than fire emission inventories on average. TROPOMI E_{CO} shares a similar seasonal variation with emission inventories with significant enhancements in August and September, while TROPOMI E_{NO2} shows an opposite trend. As a result, TROPOMI ER peaks in March–June and is significantly lower during summertime, showing the capability of distinguishing fire seasons associated with different fire types. The potential of TROPOMI ER is further examined by attributing different fire and land types. TROPOMI ER is lower for wildfires (extratropical forest fires) with an average of 0.003 ± 0.008 (0.002 ± 0.003) and higher for prescribed fires (grassland burnings) with an average of 0.017 ± 0.048 (0.019 ± 0.079). It indicates that, except for land type which is commonly used as the reference for fire categorization, fire type could be an important factor determining fire emissions. Also, TROPOMI ER could be a useful input and improve the understanding of fire characteristics in fire activity models.

Author Contributions:

Funding:

Institutional Review Board Statement:

Informed Consent Statement:

Data Availability Statement:

Acknowledgments: We acknowledge US EPA for generating the 2020 National Emissions Inventory (NEI). TROPOMI data is processed by the European Space Agency (ESA) and downloaded from the National Aeronautics and Space Administration (NASA) Goddard Earth Sciences Data and Information Services Center (GES DISC). GBBEPx data is developed by the National Oceanic and Atmospheric Administration (NOAA)/National Environmental Satellite Data and Information Service (NESDIS)/Office of Satellite and Product Operations (OSPO). FINN data is developed by the Atmospheric Chemistry Observations and Modeling (ACOM) in the National Center for Atmospheric Research (NCAR). GFAS data is developed by the European Centre for Medium-Range Weather Forecasts (ECMWF). QFED data is developed by the Global Modeling and Assimilation Office (GAMO) of NASA. We also thank the NOAA/Earth System Research Laboratories

(ESRL)/Global Systems Laboratory (GSL) and the Center for High Performance Computing (CHPC) at the University of Utah for providing archived HRRR data.

Conflicts of Interest: The authors declare no conflict of interest.

References

1. Jaffe, D.A.; O'Neill, S.M.; Larkin, N.K.; Holder, A.L.; Peterson, D.L.; Halofsky, J.E.; Rappold, A.G. Wildfire and prescribed burning impacts on air quality in the United States. *J. Air Waste Manag. Assoc.* **2020**, *70*, 583–615. https://doi.org/10.1080/10962247.2020.1749731.
2. Biswell, H. Prescribed Burning in California Wildlands Vegetation Management. Univ. of California Press, Berkeley, Calif, 1999.
3. Hardy, C.C.; Ottmar, R.D.; Peterson, J.L.; Core, J.E.; Seamon, P. Eds. *Smoke Management Guide for Prescribed and Wildland Fire*, 2001 ed.; PMS 420-2, NFES 1279; National Wildfire Coordination Group: Boise, ID, USA, 2001.
4. Borsdorff, T.; García Reynoso, A.; Maldonado, G.; Mar-Morales, B.; Stremme, W.; Grutter, M.; Landgraf, J. Monitoring CO emissions of the metropolis Mexico City using TROPOMI CO observations. *Atmos. Chem. Phys.* **2020**, *20*, 15761–15774. https://doi.org/10.5194/acp-20-15761-2020.
5. Griffin, D.; McLinden, C.A.; Dammers, E.; Adams, C.; Stockwell, C.E.; Warneke, C.; Bourgeois, I.; Peischl, J.; Ryerson, T.B.; Zarzana, K.J.; et al. Biomass burning nitrogen dioxide emissions derived from space with TROPOMI: Methodology and validation. *Atmos. Meas. Tech.* **2021**, *14*, 7929–7957. https://doi.org/10.5194/amt-14-7929-2021.
6. Jin, X.; Zhu, Q.; Cohen, R.C. Direct estimates of biomass burning NOx emissions and lifetimes using daily observations from TROPOMI. *Atmos. Chem. Phys.* **2021**, *21*, 15569–15587. https://doi.org/10.5194/acp-21-15569-2021.
7. Lama, S.; Houweling, S.; Boersma, K.F.; Eskes, H.; Aben, I.; Denier van der Gon, H.A.C.; Krol, M.C.; Dolman, H.; Borsdorff, T.; Lorente, A. Quantifying burning efficiency in megacities using the NO_2/CO ratio from the Tropospheric Monitoring Instrument (TROPOMI). *Atmos. Chem. Phys.* **2020**, *20*, 10295–10310. https://doi.org/10.5194/acp-20-10295-2020.
8. van der Velde, I.R.; van der Werf, G.R.; Houweling, S.; Eskes, H.J.; Veefkind, J.P.; Borsdorff, T.; Aben, I. Biomass burning combustion efficiency observed from space using measurements of CO and NO_2 by the TROPOspheric Monitoring Instrument (TROPOMI). *Atmos. Chem. Phys.* **2021**, *21*, 597–616. https://doi.org/10.5194/acp-21-597-2021.
9. Zhang, X.; Kondragunta, S.; da Silva, A.; Lu, S.; Ding, H.; Li, F.; Zhu, Y. The blended global biomass burning emissions product from modis and viirs observations (GBBEPX). ATBD 2019. Version 3.1. Available online: http://ospo.noaa.gov/Products/land/gbbepx/docs/GBBEPx_ATBD.pdf) (accessed on).
10. Wiedinmyer, C.; Akagi, S.K.; Yokelson, R.J.; Emmons, L.K.; Al-Saadi, J.A.; Orlando, J.J.; Soja, A.J. The Fire INventory from NCAR (FINN): A high resolution global model to estimate the emissions from open burning. *Geosci. Model Dev.* **2011**, *4*, 625–641. https://doi.org/10.5194/gmd-4-625-2011.
11. Kaiser, J.W.; Heil, A.; Andreae, M.O.; Benedetti, A.; Chubarova, N.; Jones, L.; Morcrette, J.-J.; Razinger, M.; Schultz, M.G.; Suttie, M.; et al. Biomass burning emissions estimated with a global fire assimilation system based on observed fire radiative power. Biogeosciences **2012**, *9*, 527–554. https://doi.org/10.5194/bg-9-527-2012.
12. Darmenov, A.; da Silva, A. The Quick Fire Emissions Dataset (QFED): Documentation of versions 2.1, 2.2 and 2.4. NASA Technical Report Series on Global Modeling and Data Assimilation NASA TM-2015-104606, 2015, Volume 38. Available online: http://gmao.gsfc.nasa.gov/pubs/docs/Darmenov796.pdf (accessed on).
13. Lobert, J.M.; Warnatz, J. Emissions from the Combustion Process in Vegetation. In Fire in the Environment: The Ecological, Climatic, and Atmospheric Chemical Importance of Vegetation Fires; Crutzen, P.J., Goldammer, J.G. Eds.; John Wiley & Sons Ltd.: Chichester, UK, 1993; pp. 15–37.
14. Yokelson, R.J.; Griffith, D.W.T.; Ward, D.E. Open-Path Fourier Transform Infrared Studies of Large-Scale Laboratory Biomass Fires. *J. Geophys. Res. Atmos.* **1996**, *101*, 21067–21080.
15. Burkholder, J.B.; Sander, S.P.; Abbatt, J.P.D.; Barker, J.R.; Huie, R.E.; Kolb, C.E.; Kurylo, M.J.; Orkin, V.L.; Wilmouth, D.M.; Wine, P.H. *JPL Publication 15-10 Chemical Kinetics and Photochemical Data for Use in Atmospheric Studies, 18*; NASA Jet Propulsion Laboratory: 2015. Available online: https://jpldataeval.jpl.nasa.gov/pdf/JPL_Publication_15-10.pdf (accessed on).
16. Goldberg, D.L.; Anenberg, S.C.; Kerr, G.H.; Mohegh, A.; Lu, Z.; Streets, D.G. TROPOMI NO_2 in the United States: A detailed look at the annual averages, weekly cycles, effects of temperature, and correlation with surface NO_2 concentrations. *Earth'S Future* 2021, 9, e2020EF001665. https://doi.org/10.1029/2020EF001665.
17. Liu, Y.Q. Variability of wildland fire emissions across the contiguous United States. *Atmos. Environ.* **2004**, *38*, 3489–3499. https://doi.org/10.1016/j.atmosenv.2004.02.004.
18. Liu, X.; Huey, L.G.; Yokelson, R.J.; Selimovic, V.; Simpson, I.J.; Müller, M.; Jimenez, J.L.; Campuzano-Jost, P.; Beyersdorf, A.J.; Blake, D.R.; et al. Airborne measurements of western U.S. wildfire emissions: Comparison with prescribed burning and air quality implications. *J. Geophys. Res. Atmos.* 2017, 122, 6108– 6129. https://doi.org/10.1002/2016JD026315.
19. Yokelson, R.J.; Karl, T.; Artaxo, P.; Blake, D.R.; Christian, T.J.; Griffith, D.W.T.; Guenther, A.; Hao, W.M. The Tropical Forest and Fire Emissions Experiment: Overview and airborne fire emission factor measurements. *Atmos. Chem. Phys.* **2007**, *7*, 5175–5196. https://doi.org/10.5194/acp-7-5175-2007.
20. Akagi, S.K.; Yokelson, R.J.; Wiedinmyer, C.; Alvarado, M.J.; Reid, J.S.; Karl, T.; Crounse, J.D.; Wennberg, P.O. Emission factors for open and domestic biomass burning for use in atmospheric models. *Atmos. Chem. Phys*. **2011**, *11*, 4039–4072. https://doi.org/10.5194/acp-11-4039-2011, 2011.

21. Andreae, M.O.; Merlet, P. Emission of trace gases and aerosols from biomass burning. *Global Biogeochem. Cycles* **2001**, *15*, 955–966. https://doi.org/10.1029/2000GB001382.
22. McMeeking, G.R.; Kreidenweis, S.M.; Baker, S.; Carrico, C.M.; Chow, J.C.; Collett Jr. J. L.; Hao, W.M.; Holden, A.S.; Kirchstetter, T.W.; Malm, W.C.; Moosmüller, H.; et al. Emissions of trace gases and aerosols during the open combustion of biomass in the laboratory. *J. Geophys. Res.* **2009**, *114*, D19210. https://doi.org/10.1029/2009JD011836.